International Journal of Modern Physics B
Vol. 33 (2020) 2040067 (8 pages)

DOI: 10.1142/S0217979220400676

Surface modification of TiO_2 for visible light photocatalysis: Experimental and theoretical calculations of its electronic and optical properties

Dessy Ariyanti[*,†,‖], Surayya Mukhtar[‡,**], Nisar Ahmed[§,††], Zhuofeng Liu[¶,‡‡], Junzhe Dong[†,§§] and Wei Gao[†,¶¶]

[*] *Department of Chemical Engineering, Universitas Diponegoro, Semarang 50275, Indonesia*

[†] *Department of Chemical and Material Engineering, The University of Auckland, Auckland 1142, New Zealand*

[‡] *Department of Physics, Allama Iqbal Open University, Islamabad, Pakistan*

[§] *Department of Physics and Applied Mathematics, Pakistan Institute of Engineering and Applied Sciences, Nilore, Islamabad, Pakistan*

[¶] *College of Aerospace and Materials Engineering, National University of Defence Technology, Changsha 410073, P. R. China*

[‖] *dessy.ariyanti@che.undip.ac.id*
[**] *surayyaafridi@yahoo.com*
[††] *nisarbinwali@gmail.com*
[‡‡] *liuzhuofeng@hotmail.com*
[§§] *jdon296@aucklanduni.ac.nz*
[¶¶] *w.gao@auckland.ac.nz*

Received 30 April 2019
Accepted 20 August 2019
Published 26 December 2019

Surface modification has been used as a method to create defects on TiO_2 materials, which can improve their desirable properties. In this paper, defected TiO_2 nano-powder was successfully synthesized by chemical reduction using $NaBH_4$ as the reducing agent at 300–400°C under argon atmosphere. High defect concentration can be produced by increasing process temperature. The modified TiO_2 shows good visible light absorption and photocatalytic activity on degradation of Rhodamine B (4–9 times higher than the pristine TiO_2) with the visible light irradiation. Further XPS analysis and theoretical studies using full potential linearized augmented plane wave (FP-LAPW) method as implemented in wien2k code revealed the existence of oxygen vacancy and Ti^{3+} in the modified samples. These types of defects were responsible for the modifications of the electronic and optical properties of TiO_2, resulting in the improved photocatalytic activity in visible light irradiation.

[‖] Corresponding author.

Keywords: $NaBH_4$ reduction; defect; density functional theory; TiO_2; visible light absorption.

PACS number: 78.20.Bh

1. Introduction

TiO_2 is a wide bandgap semiconductor (3.0–3.2 eV) that can be used as photocatalyst.[1] It requires ultraviolet radiation (290–400 nm) to excite electrons from the valance band, not visible or fluorescent light,[2] which limit their application in utilizing major solar light spectrum. In order to enable light absorption in the visible region and to improve the photo-efficiency of TiO_2, doping TiO_2 with nonmetals (such as C, N, S or F), metals (such as Fe, Cr or V) or metal oxides (such as V_2O_5, ZrO_2 or WO_3) has been reported. Hybrid materials combining TiO_2 with carbon materials such as carbon nanotubes, activated carbons or TiO_2-carbon microspheres were also investigated for the same propose.[3–5] In addition, new photocatalytic materials have been developed to achieve higher activities than TiO_2-based photocatalysts; but the success cases for practical applications are few. One of the most viable and practical approaches in developing better photocatalysts is to use self-modify TiO_2 processes, including surface modification.

In this paper, surface modification has been conducted by chemical reduction using $NaBH_4$ to create defects in pristine TiO_2 powder. $NaBH_4$ is an inorganic compound that can be used as a versatile reducing agent. Thermal decomposition of $NaBH_4$ releases active hydrogen that is favorable for defect introduction to the surface of semiconductor.[6] The effect of temperature was studied in correlation to its optical and electronic properties. The full potential linearized augmented plane wave (FP-LAPW) method within density functional theory (DFT) was employed to investigate the effect of oxygen vacancy on the optical and electronic properties of the modified samples.

2. Experimental Details

2.1. *Preparation of modified TiO_2 and sample characterization*

Anatase TiO_2 (Sigma Aldrich Co. size <25 nm) and reduction agent $NaBH_4$ (ECP Ltd.) were used as the starting material. First, 0.75 g $NaBH_4$ was mixed with 2.0 g TiO_2, heating then applied for 60 min in a furnace under Ar to 300–400°C (labelled X300, X350 and X400, cooled down, washed with DI water, and dried at 110°C.[7] The prepared samples were then characterized by XRD, UV-Vis-NIR and XPS.

2.2. *Photocatalytic degradation of organic pollutant*

Photocatalytic activity was evaluated by monitoring the decomposition of RhB in an aqueous solution under visible light irradiation (ULTRA VITALUX 300 W 230 V E27 with UV cut-off filter). Photocatalyst (50 mg) was mixed with RhB

solution (50 mL, 5 ppm), followed by 30 min stirring in dark to reach the adsorption equilibrium. Two milliliters were taken every time to filter by 0.2 mm PVDF syringe filter. The concentration of RhB was determined with a UV-Vis spectrophotometer by the peak intensity at 553 nm.

2.3. *Method for theoretical calculations*

The calculations were first carried out on the primitive unit cell of TiO_2 in anatase phase. The $2 \times 2 \times 2$ 96-atom anatase supercell was used to construct TiO_2 systems with oxygen vacancy V_o (concentration was set at 4.1%) and to calculate the V_o energy formation using FP-LAPW method as implemented in wien2k code.[8] The wavefunction for core states is taken as atomic like function, while for the valence states, it is considered as plane waves. The muffin-tin radius for core states is denoted as R_{MT}. Outside R_{MT}, valence states are accounted. In this work, nonoverlapping R_{MT} for Ti and O atoms were 1.93 and 1.75 a.u, respectively. Energy convergence criteria were set at 10^{-4} eV. For calculation of electronic and optical properties, a k mesh of 36 points was sampled in the irreducible Brillouin zone (IBZ). The maximum cut-off for the plane wave $k_{\max}$ is 6.5. Exchange correlations effects are considered under generalized gradient approximation (GGA), GGA+U (with U as Hubbard potential, set as 10.303 eV) and Tran–Blaha modified Becke–Johnson (TB-mBJ) approximation.

3. Results and Discussion

3.1. *Structures features and physical properties*

As shown in Fig. 1(a), small changes such as peak boardening and reduction of the peak intensity were observed in the XRD peaks of the modified TiO_2 in comparison to the pristine one. The diffraction peaks of all samples were assigned for TiO_2 anatase (JCPDS card 78-2486) indicating that all samples have the same crystalline structure (anatase). Only peak intensity was reduced gradually with increasing. The deformation of cystalline lattice may occur and defect be created, thus resulting in low peak intensity.[7] Table 1 shows the crystallite size and lattice strain of the pristine and $NaBH_4$ modified TiO_2 estimated by Debye–Scherrer and Stokes–Wilson equations. As the temperature of reduction process gets higher, the crystallite size slightly reduces (from 63.5 to 48.8 nm), and the lattice strain slightly increases (0.010–0.012). Strain broadening is often triggered by lattice imperfection, including vacancies, interstitials and substitutions.[9]

Figure 1(b) depicts the optical properties of pristine and modified TiO_2 samples which are represented by the light absorption behavior. The absorbance intensity from 400 to 800 nm increased as the $NaBH_4$ treatment temperature increased. All modified samples were able to absorb visible light while pristine TiO_2 has no absorption. The enhancement of light visible light absorption in TiO_2 were also reported in Refs. 6 and 10–13.

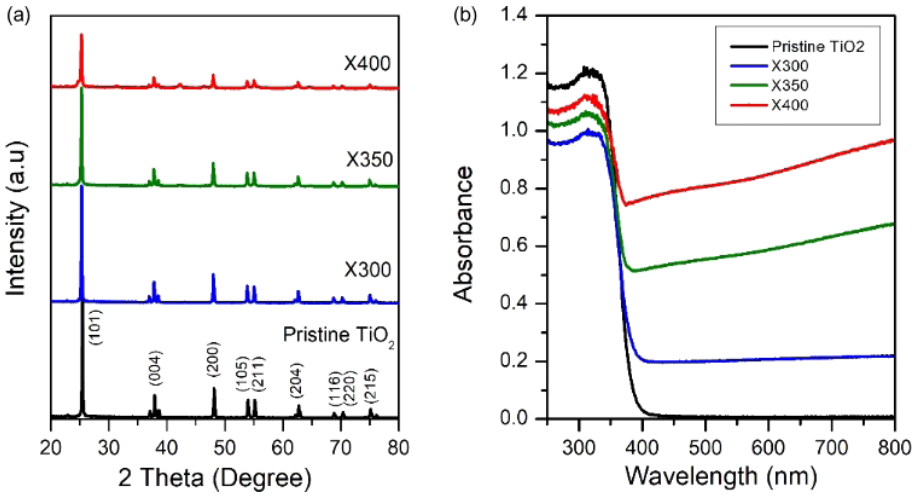

Fig. 1. (Color online) (a) XRD pattern and (b) UV-Vis spectrum of pristine and $NaBH_4$ modified TiO_2.

Table 1. Crystallite size and lattice strain of pristine and $NaBH_4$ modified TiO_2.

Samples	FWHM	Peak position	Crystallite size (nm)	Lattice strain
TiO_2 pristine	0.128	25.41	63.5	0.00991
X300	0.126	25.22	61.6	0.00981
X350	0.134	25.26	60.2	0.01044
X400	0.157	25.24	48.8	0.01224

Table 2. Percentage area of O 1*s*.

Sample	O 1*s* (Ti-O) (%)	O 1*s* (O-H) (%)
Pristine TiO_2	68.10	31.90
X300	62.65	37.35
X350	56.26	43.74
X400	44.54	56.46

Figure 2 compares the XPS spectra of Ti 2*p* of pristine and modified TiO_2 at different temperatures. Ti^{4+} and Ti^{2+} were detected in all samples, representing the same state of Ti atoms that existed in these samples. However, additional peak of Ti^{3+} was detected in X350 [Fig. 2(c)], indicating the existence of defects. Hydroxide (O-H) and Ti (Ti-O) in the oxygen state (O 1*s*) were also detected. The presence of hydroxide is predictable as the defect formation involves the attraction of active hydrogen with the oxygen in the lattice structures, thus it can be associated with the surface defects and oxygen vacancies.[14] Table 2 shows the percentage of O 1*s* (H-O) in the sample, which increases gradually with increasing temperature. High percentage of O 1*s* (H-O) indicates the existence of distortion on the TiO_2 surface and more severe conditions compared to the distortion in bulk.[7]

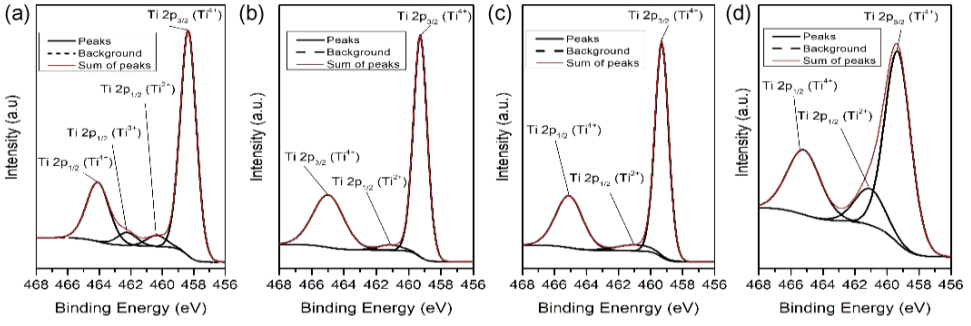

Fig. 2. (Color online) XPS spectra of Ti 2*p*: (a) pristine TiO_2, (b) X300, (c) X350 and (d) X400.

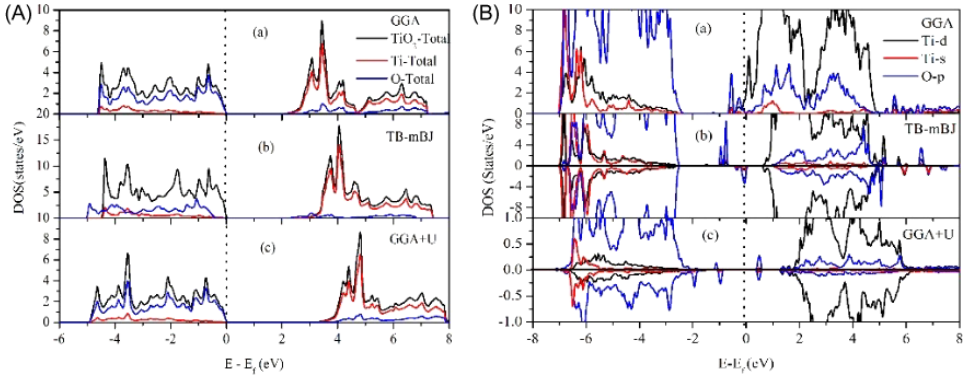

Fig. 3. (Color online) Density of states of (a) pristine and (b) defected TiO_2 with oxygen vacancy V_o.

XPS also indicate the electronic band position of the materials (valence band). The valence band maximum (VBM) is estimated by a linear extrapolation of the peak to the baseline.[15] The pristine TiO_2 have a band edge position of 1.7 eV below the Fermi energy. Meanwhile, the band edge of modified TiO_2 were slightly lower by 0.1; 0.4 and 0.2 eV for X300; X350 and X400, respectively. There is a possibility of the formation of an extra band between the Fermi level (0 eV) and the top of the VB triggered by the defect of Ti^{3+} and oxygen vacancies.[15] To confirm the formation of extra band of the modified TiO_2, the theoretical calculation based on FP-LAPW DFT was conducted and discussed in Sec. 3.3.

3.2. *Photocatalytic activity*

Table 3 presents the kinetic constant of pristine and modified TiO_2 on RhB degradation under visible light. Sample X350 has the highest degradation rate of $k = 0.0018$/min, followed by X300 and X400 with $k = 0.0011$ and 0.0008/min, respectively. The pristine TiO_2 has the lowest degradation rate as it does not absorb visible light. As X400 has higher oxygen vacancies O 1*s* (H-O), it has lower

Table 3. Kinetics constant of RhB degradation under visible light.

Catalyst	Kinetics constant (min^{-1})	R^2
Pristine TiO_2	0.0002	0.9601
X300	0.0011	0.9648
X350	0.0018	0.9811
X400	0.0008	0.9864

photocatalytic activity compared to X300 and X350. This can be explained by the possibility of samples having different type and concentration of defects. By decreasing the relative defect concentration of bulk to surface in the TiO_2, the photocatalytic efficiency is significantly enhanced.[14,16]

3.3. *Theoretical studies*

The calculated bandgap energy for pristine TiO_2 by using GGA, GGA+U and TB-mBJ approximations is 2.015, 3.246 and 2.872 eV, respectively. Figure 3(a) shows the total density of states for anatase TiO_2 unit cell. Based on Fig. 3(a), the conduction band is made up of Ti-3d valence states while O-2p states contribute in the formation of the valence band. The supercell model, oxygen vacancy V_o, was created; and the effect of V_o on the bandgap and state of density of states was investigated. Density of states (DOS) of Ti-d, Ti-s and O-p states are plotted [Fig. 3(b)]. It shows the new localized states between the conduction band and valence band are O-2p states which are created due to the V_o defect. TB-mBJ gives bandgap $\sim$0.7 eV in spin up channel and $\sim$0.446 eV in spin down channels. The conduction band and valence band both shift to the lower energy levels and become narrower. DOS shows that new O-2p states are located at 1.1 eV above the VBM due to V_o defect. Similar to GGA, these localized energy states in the valence band act as the trap centers for photoexcited holes.

GGA+U approximation depicts a different picture as compared to GGA and TB-mBJ schemes. The bandgap is improved and gives $\sim$1.5 eV in spin down channel whereas it reduced to $\sim$0.426 eV in the spin up channel. The energy states due to V_o are located in the conduction band and valence band. These are O-2p states which form shallow levels at the CBM and localized energy states at 1.5 eV below the conduction band. In the valence band, they form shallow donor energy levels at VBM edge and localized energy states at $\sim$0.7 eV above the VBM. The possible explanation of this behavior is that V_o acts like donor impurity with a charge state +2. With the creation of V_o, three O-2p states but four electrons were removed, which are responsible for the valence band formation. Now, two Ti-3d electrons need to transfer from the conduction band to valence band to fill the O-2p_y and O-2p_z states in the pristine TiO_2 unit cell, residing in the conduction band.

These unpaired Ti-3d electrons behave like free electrons in the conduction band, and are responsible for the n-type conductivity in TiO_2. Reports cited the effect

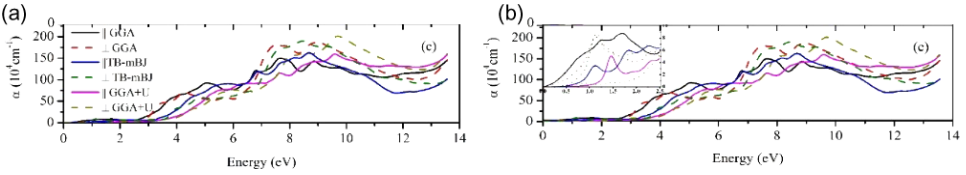

Fig. 4. (Color online) Absorption coefficient spectra of (a) pristine and (b) defected TiO_2.

of V_o defects on the photocatalytic activity.[17] The presence of oxygen vacancies in TiO_2 can increase or reduce the photocatalytic activity depending on the factors of the concentration of V_o, oxygen vacancy at the surface or in the bulk. They provide trap centers for electrons and holes, either increase or decrease the electron–hole recombination rate. It is also reported that the electrons can easily be photo-excited to these localized states by visible light absorption and cause an increase in the photocatalytic activity.[17]

The threshold energy for absorption is closely related to the optical bandgap of the material. For pristine TiO_2, it is calculated as 2.3–2.5, 3.2–3.5 and 3.5–4.0 eV in parallel and perpendicular directions of incident photons with GGA, TB-mBJ and GGA+U approximations, respectively [Fig. 4(a)]. Figure 4(b) shows the light absorption in the visible energy range of ∼0.5–2.5 eV for defected TiO_2 and confirmed by the experimental results presented in Fig. 2. Although the absorption in visible light is very low compared to the UV region, the photocatalytic activity is significantly enhanced by V_o defects, as shown in Table 3.

4. Conclusion

Defects have been successfully introduced to the pristine TiO_2 via $NaBH_4$ treatment. Its concentration can be controlled by temperature. The modified TiO_2 has good visible light absorption and high photocatalytic activity towards RhB degradation (4–9 times higher than pristine TiO_2). This may come from the formation of V_o and Ti^{3+}. Theoretical calculations confirm the presence of extra energy states created by V_o. The bandgap is reduced in the TiO_2 with V_o defects as compared to pristine TiO_2. These changes lead to a disordered layer and a broad visible light absorption which is in line with the experimental findings.

References

1. A. Fujishima and K. Honda, *Nature* **238**, 37 (1972).
2. X. Wang *et al.*, *J. Hazard. Mater.* **262**, 16 (2013).
3. M. Sillanpää, M. C. Ncibi and A. Matilainen, *J. Environ. Manage* **208**, 56 (2018).
4. A. Fujishima, X. Zhang and D. A. Tryk, *Surf. Sci. Rep.* **63**, 515 (2008).
5. X. Chen, L. Liu and F. Huang. *Chem. Soc. Rev.* **44**, 1861 (2015).
6. H. Tan *et al.*, *Nanoscale* **6**, 10216 (2014).
7. D. Ariyanti *et al.*, *Mater. Chem. Phys.* **199**, 571 (2017).

8. P. K. S. Blaha *et al.*, WIEN2k: An augmented plane wave plus local orbitals program for calculating crystal properties (2001).
9. D. Balzar, *J. Res. Natl. Inst. Stand. Technol.* **98**, 321 (1993).
10. J. Dong *et al.*, *ACS Appl. Mater. Interfaces* **6**, 1385 (ẏ2014).
11. H. Wang *et al.*, *Catal. Commun.* **60**, 55 (2015).
12. G. Zhu *et al.*, *ChemCatChem.* **7**, 2614 (2015).
13. T. Lin *et al.*, *Energy Environ. Sci.* **7**, 967 (2014).
14. J. Yan *et al.*, *Phys. Chem. Chem. Phys.* **15**, 10978 (2013).
15. S. Pan *et al.*, *J. Mater. Chem. A* **3**, 11437 (2015).
16. M. Kong *et al.*, *J. Am. Chem. Soc.* **133**, 16414 (2011).
17. X. Pan *et al.*, *Nanoscale* **5**, 3601 (2013).